



Triboelectric immunotherapy using electrostatic-breakdown induced direct-current

Haimei Li^{1,2,3,8,#}, Chaoyu Chen^{4,#}, Zichen Wang¹, Yiman Huang³, Guangqin He^{1,2}, Yi Liu^{3,5,6,*}, Peng Jiang^{1,2,8,*}, Zhong Lin Wang^{7,*}

¹ Department of Orthopedics Trauma and Microsurgery, Zhongnan Hospital of Wuhan University, School of Pharmaceutical Sciences, Wuhan University, Wuhan 430071, China

² Key Laboratory of Combinatorial Biosynthesis and Drug Discovery (MOE), Wuhan University, Wuhan 430071, China

³ Key Laboratory of Coal Conversion and New Carbon Materials of Hubei Province & Institute of Advanced Materials and Nanotechnology, College of Chemistry and Chemical Engineering, Wuhan University of Science and Technology, Wuhan 430081, China

⁴ Engineering Research Center of Knitting Technology, Ministry of Education, College of Textile Science and Engineering, Jiangnan University, Wuxi 214122, China

⁵ School of Chemical and Environmental Engineering, Wuhan Polytechnic University, Wuhan 430023, China

⁶ State Key Laboratory of Separation Membrane and Membrane Process & Tianjin Key Laboratory of Green Chemical Technology and Process Engineering, School of Chemistry, Tiangong University, Tianjin 300387, China

⁷ Beijing Institute of Nanoenergy and Nanosystems, Chinese Academy of Sciences, Beijing 100083, China

⁸ Hubei Jiangxia Laboratory, Wuhan 430200, China

Electrical stimulation is a promising technique for drug-free treatment of complex malignant tumors because it can directly kill tumor cells and induce immunotherapy, avoiding the risk of drug-related side effects, toxicity, adverse reactions, drug dependence, drug resistance, etc. Herein, a drug-free tumor therapy strategy, defined as “Triboelectric Immunotherapy”, is invented to directly damage tumor cells and recruit immune cells by applying pulsed direct-current (DC) generated from a small size fabric DC triboelectric nanogenerator (DC-TENG). The pulsed DC is generated by coupling triboelectrification effect and electrostatic breakdown effect. The electrical stimulation can promote immunogenic cell death (ICD) of 4T1 cells to release damage-associated molecular patterns that attract dendritic cells to aggregate in tumors and present exposed abundant antigens to T cells, activating T cells-mediated adaptive immunity response to further inhibit tumor growth. Importantly, tissue structures such as blood vessels were preserved during electrical stimulation, allowing cytokines to accumulate to the tumor site through blood supply, significantly inhibiting the growth of 4T1 solid tumors and effectively prolonging survival. This work provides a highly efficient, cost-effective and safe solution for miniaturized wearable tumor treatment system.

Keywords: Triboelectric nanogenerator; Triboelectric immunotherapy; Drug-free; Immunotherapy

Introduction

The development of drug-free treatment of complex malignant tumors is of great importance for future clinical application because it avoids the risks of drug-related side effects, toxicity, adverse reactions, drug dependence, drug resistance, etc [1,2].

* Corresponding authors.

E-mail addresses: Liu, Y. (yiliu@whu.edu.cn), Jiang, P. (jiangpeng@whu.edu.cn), Wang, Z.L. (zhong.wang@mse.gatech.edu).

Haimei Li, Chaoyu Chen contribute equally to this work.

Electrical stimulation is a promising technique for drug-free tumor treatment because it can directly kill tumor cells and induce immunotherapy [3–5]. Furthermore, electrical stimulation therapy can also be combined with the current rapidly developing wearable health monitoring technology to build the next generation of miniaturized wearable medical devices integrating diagnosis and treatment capabilities. Clinical treatment has proved that electrical stimulation under high voltage can cause permanent damage to tumor cells and produce direct cytotoxic effects. At the same time, the preservation of important structures such as blood vessels can also enable immune cells to migrate into tumors along with blood and lymphatic vessels, enabling the combination of electrical stimulation and immunotherapy, which is critical for tumor suppression [6–9]. It has been reported that the death of tumor cells stimulated by electricity can be transformed from non-immunogenic to immunogenic, mediating the body's anti-tumor immune response, that is, immunogenic cell death (ICD), which results in the release of massive tumor antigens and damage-associated molecular patterns (DAMPs), attracting dendritic cells recruit at tumor site [10,11]. Importantly, dendritic cells that have taken up tumor antigens migrate to tumor-draining lymph nodes (TDLNs) to complete antigen presentation to T cells, thereby realizing the activation of cytotoxic T cell-mediated adaptive immune responses [12,13]. In this regard, the advantage of using electrical stimulation to induce ICD without interfering with the migration of immune cells to tumors will have great application prospects in tumor therapy [14,15].

Electroporation is one of the most important electrical-assisted therapy techniques, including irreversible electroporation (IRE), electrochemotherapy (ECT), calcium electroporation [16–18]. IRE is a well-developed tumor ablation treatment strategy that uses high-voltage short pulses to cause nano-scale perforation of the cell membrane and lead to cell apoptosis [19]. Currently, a commercial IRE system, called as “NanoKnife”, has been approved by Food and Drug Administration (FDA) to treat soft tissue tumor [20,21]. Recently, nanosecond pulsed stimulation has aroused extensive attention because of its extremely short pulse durations (ns) and high electric field strength (kV/cm) along with non-thermal effects [22]. Although these electrical-assisted therapy techniques have good potential and some of them have been implemented in clinical trials [23–25], they often require expensive and bulky therapeutic equipment, limiting their portability and wearability. As well known, miniaturized wearable medical devices are the trend of next-generation medical devices [26,27]. Moreover, the extremely high voltage during these electrical-assisted treatment increases the operation risk.

Triboelectric nanogenerator (TEG) is a promising power source for wearable and implantable biomedical device that convert bio-mechanical energy into electricity through the coupled effects of triboelectrification and electrostatic induction [25–29]. In recent years, TEG have been widely used in drug delivery [30], wound repair [31], and prevention of cancer metastasis. Moreover, the output from TEG can induce cell electroporation, which can be applied to drug delivery [32]. Recently, TEG with pulsed direct-current (DC) output were fabricated by coupling the triboelectrification effect and electrostatic breakdown

effect [33,34]. These DC-TEG have great potential in electrical stimulation-assisted tumor ablation treatment. First, the DC-TEG can generate pulsed DC, which is similar to that used in previously reported electrical stimulation-assisted tumor therapy. Second, the DC-TEG can be fabricated with flexible materials (such as textile), and can generate sufficiently strong currents in small dimensions, making them ideal for miniaturized wearable tumor treatment devices [35,36]. Finally, DC-TEG is a safe power source that avoids the operation risks associated with high voltages in conventional power supplies. To date, DC-TEG have not been applied to tumor therapy.

Herein, a drug-free tumor therapy strategy called “Triboelectric Immunotherapy” is invented to directly damage tumor cells and recruit immune cells by applying pulsed direct-current generated from a fabric DC-TEG (Fig. 1a). A small fabric DC-TEG (6.8 cm × 7 cm) was applied to generate sufficiently high DC output to directly induce immunogenic cell death of tumor cells. Notably, important tissue structures, such as blood vessels, were not damaged during the electrical stimulation. Interestingly, a series of DAMPs generated during this process can enter the extracellular environment, which increases dendritic cells infiltration at the tumor site and migrates to TDLNs, where tumor antigens and co-stimulatory molecules are presented to T cells. Subsequently, T cells differentiate into cytotoxic CD4⁺/CD8⁺ T cells, and ultimately trigger T cell-mediated antitumor immunity. It has shown excellent tumor inhibition ability and biological safety, effectively prolonging the life cycle of patients, and has broad prospects in the field of tumor therapy. Furthermore, in order to precisely insert the electrical stimulation needle into the tumor site, tumor-targeting Ag₂S quantum dots (QDs) with 1170 nm emission were injected to guide the insertion operation with second near-infrared (NIR-II) fluorescence imaging. This work provides a highly efficient, cost-effective and safe solution for miniaturized wearable tumor treatment system.

Results and discussion

Output performance of the fabric DC-TEG

The schematic of experimental setup of “Triboelectric Immunotherapy” is shown in Fig. 1A. Our proposed system consists of a sliding mode fabric DC-TEG and two electrical stimulation needles that penetrate into the tumor tissues. The fabric DC-TEG is constructed from a piece of textile composed of PA nonconductive yarns and PA conductive yarns [35], where the conductive yarns are separated by nonconductive yarns to serve as electrostatic breakdown electrodes and frictional electrodes (Fig. S1, Supporting Information). To generate pulsed direct current, the fabric DC-TEG should in contact with a polytetrafluoroethylene (PTFE) triboelectric layer and slide periodically (As shown in Movie S1, Supporting Information). The working principle of fabric DC-TEG is illustrated in Fig. S2. Since the fabric TEG is composed of multiple repeating woven units, for better understanding, the working principle is described based on one woven unit. PTFE is a highly negative electret material, when the frictional electrodes is in sliding contact with PTFE, PTFE will be negatively charged due to the triboelectrification effect, and can hold the negative charges in an extended period of time. Correspondingly, the frictional elec-

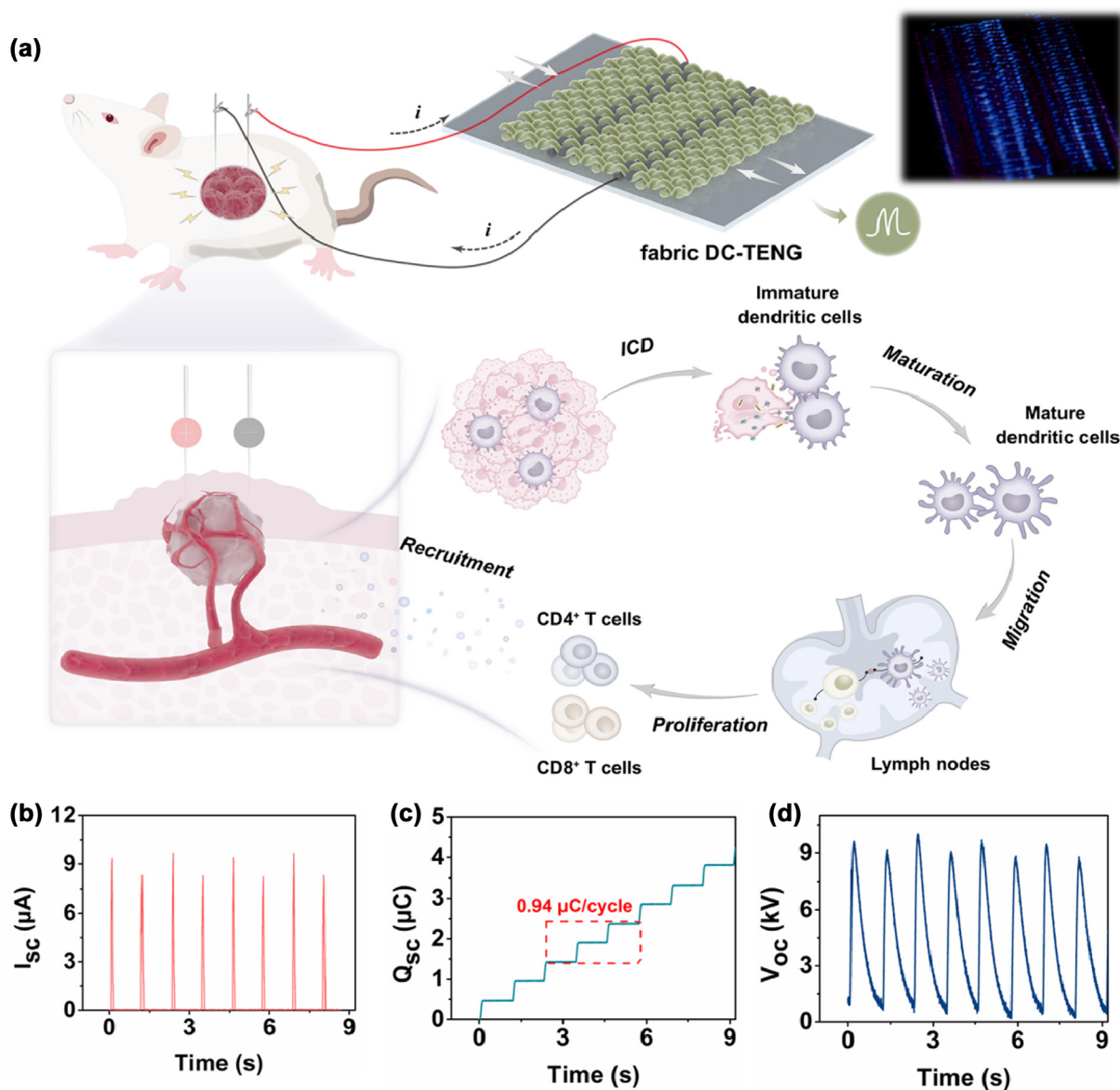


FIGURE 1

Schematic diagram and performance characterization of fabric DC-TENG. (a) Schematic illustration of the “Triboelectric Immunotherapy” system and the pulsed direct-current induced ICD-mediated immune recruitment and initiation of adaptive immune response. (b) Short-circuit current (I_{sc}), (c) short-circuit charge transfer (Q_{sc}) and (d) open-circuit voltage (V_{oc}) of fabric DC-TENG.

trodes will be positively charged (Stage i of Fig. S2, Supporting Information). When the fabric DC-TENG is gradually moves forward, partial positive charges will flow to the electrostatic breakdown electrode, forming an extremely high electrostatic field between the electrostatic breakdown electrode and negatively charged PTFE film (Stage ii of Fig. S2, Supporting Information). Once the electrostatic field exceeds the dielectric strength of the air between them, air breakdown occurs, resulting in a discharge process between the electrostatic breakdown electrode and the PTFE, and generating pulsed current (Stage iii of Fig. S2, Supporting Information) [37]. When the fabric DC-TENG moves backward, there is no charges in between the electrostatic breakdown electrode and PTFE film, therefore, air breakdown will not happen and no current generated (Stage iv of Fig. S2, Supporting Information). The air breakdown phenomenon during the sliding process can be directly observed

by the photograph with 30 s exposure taking in a dark room (as shown in the upper right of Fig. 1a). In this work, a small fabric DC-TENG consisting of 8 repeating woven units (6.8 cm \times 7 cm) was applied, its open-circuit voltage (V_{oc}), short-circuit current (I_{sc}), and short-circuit charge transfer (Q_{sc}) can achieve about 8000 V, 9 μA , and 0.94 μC per cycle, respectively (Fig. 1b-d) [35].

Electrical stimulation-triggered ICD in vitro

Electrical stimulation induced cell death driven by fabric DC-TENG was evaluated by classical MTT experiments [38,39]. The experimental setup is shown in Fig. 2a, the cell suspension was placed in an electroporation cup, which was connected with the two electrodes of fabric DC-TENG, and continuously stimulated for different times [40]. After static incubation for 24 h, the cell viability was determined by the MTT assay (Fig. 2b).

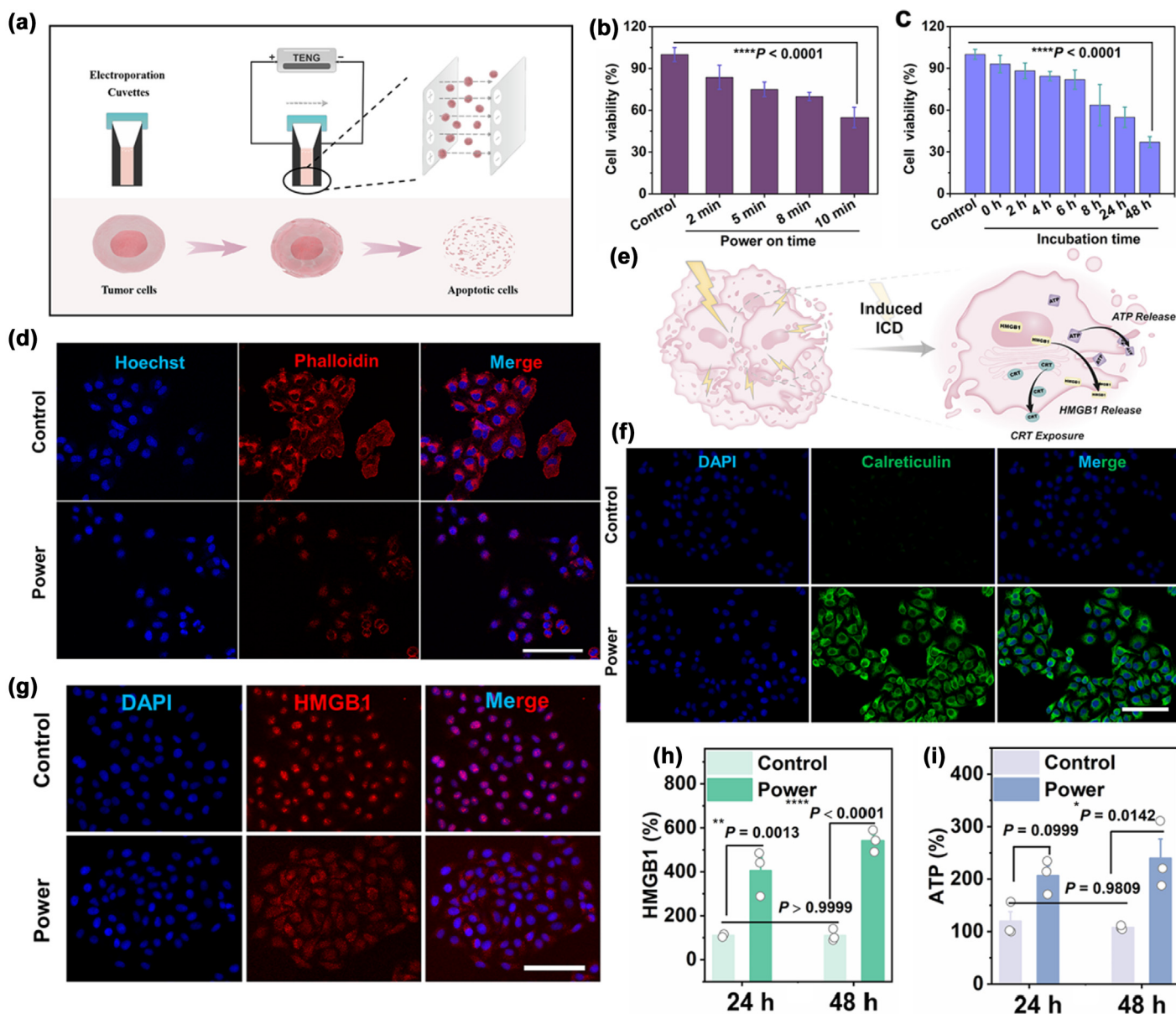


FIGURE 2

Electrical stimulation-induced ICD driven by fabric DC-TENG at the cellular level. (a) Schematic illustration of the procedure to achieve electrical stimulation in 4T1 cells using an electroporation cup. Current intensity: 9 μ A. (b) Cell viability of 4T1 cells incubated for 24 h under different electrical stimulation times. (c) Cell viability of 4T1 cells after electrical stimulation for 10 min under different incubation times. (d) Phalloidin-stained (red) fluorescence microscopy images of F-actin in 4T1 cells. Nuclei were labeled with Hoechst 33342. Scale bar: 100 nm. (e) Schematic illustration of immunogenic cell death that occurs in cells under electrical stimulation. Fluorescence microscopy images of (f) calreticulin (green fluorescence) and (g) HMGB1 (red fluorescence) expressed by 4T1 cells under electrical stimulation. Scale bar: 100 nm. Histogram of (h) HMGB1 and (i) ATP content released to the 4T1 cells external environment with different treatments after 24 h. All data are presented as the mean values with error bars (standard deviations, \pm s.d.) from three biologically independent samples ($n = 3$). The statistical significance analysis was determined using Student's t-test (two-group analysis) or one-way analysis of variance (ANOVA) (multigroup analysis). n.s. not significant, * $p < 0.1$, ** $p < 0.01$, *** $p < 0.001$, **** $p < 0.0001$.

The results show that the survival rate of tumor cells gradually decreased with the prolongation of electrical stimulation time, and the cell viability was decreased to 54.77 % with 10 min electrical stimulation. Subsequently, the electrical stimulation time was fixed at 10 min, and the cell viabilities at different incubation times were measured (Fig. 2c). The survival rate of tumor cells gradually decreased with the prolongation of incubation time, which proved that TENG electrical stimulation-mediated cell death did not occur instantaneously, but occurred continu-

ously after the termination of electrical stimulation. In addition, the electrical stimulation also has a significant killing effect on other types of tumor cells such as Hela cells and NALM6 cells (Fig. S4, Supporting Information). Notably, the electrical stimulation only caused slight damage to normal cells (293 cells and COS7 cells) (Fig. S5, Supporting Information), which proves the good biological safety of this therapy. Then, the F-actin of cells was stained with phalloidin to explore the effect of electrical stimulation on the cytoskeleton [41,42]. As shown in Fig. 2d,

the untreated group (Control) had intact cell morphology and displayed red fluorescence of the cytoskeleton around the cells. In contrast, electrical stimulation treatment resulted in the degradation of cellular actin filaments and decreased the red fluorescence, demonstrating that fabric DC-TENG-driven electrical stimulation has a significant disruptive effect on the cytoskeleton [41,42]. Moreover, it has been reported that electrical stimulation of tumor cells can trigger ICD, inducing tumor cells to release large amounts of tumor-associated antigens and DAMPs (such as calreticulin ectopic) exposed on the surface of dying cells, and high-mobility group box 1 (HMGB1) migrates from the nucleus, which accompanies the release of ATP into the extracellular milieu (Fig. 2e) [6,11,43–45]. As shown in Fig. 2f, electrical stimulation induced the expression of CRT (strong green fluorescence) on the surface of 4T1 cells, which is an “eat me” signal that activates the phagocytosis of dead cancer cells and debris by antigen-presenting cells (APCs) [46]. Besides, electrical stimulation also allows HMGB1 to leak from the nucleus to the outside of cells as a “danger” signal (Fig. 2g), acting as a natural adjuvant that stimulates the maturation of dendritic cells [47]. The enzyme-linked immunosorbent assay (ELISA) further proved that the content of HMGB1 in the extracellular environment of cells in the electrical stimulation group (Power group) is significantly higher than that of the control group (Fig. 2h). Interestingly, the extracellular ATP content assay in the power group show a significant increase in ATP secretion (Fig. 2i), releasing a “find me” signal to the outside world, which is a key signal for attracting the recruitment and maturation of dendritic cells [48,49]. These results indicate that the pulsed electrical stimulation driven by fabric DC-TENG can effectively trigger massive immunogenic cell death and activate antitumor immune responses.

NIR-II fluorescence imaging-guided triboelectric immunotherapy in vivo

For electrical stimulation tumor therapy, the position of the needle on the tumor will significantly affect the therapeutic effect, so imaging methods are needed to guide the needle insertion operation, especially for tumors in deep tissues that cannot be seen with the naked eye [15,19,50]. NIR II fluorescence imaging is considered a promising technique for guiding surgery in clinical because of its excellent temporal and spatial resolution [39,51,52]. Fig. 3a shows the schematic diagram of electrical stimulation needle insertion under the guidance of NIR II fluorescence imaging. In this work, tumor-targeting 4T1 cell membrane-coated Ag₂S QDs (Ag₂S@CM) with NIR II emission (1170 nm) were synthesized for the proof-of-concept demonstration of NIR II imaging guided needle insertion (Fig. 3b, c). The Ag₂S@CM exhibits extremely low cytotoxicity and excellent stability, demonstrating the outstanding biosafety of Ag₂S@CM (Figs. S6 and S7, Supporting Information). Fig. 3d shows the NIR II imaging of tumor-bearing mice before and intravenous injection of Ag₂S@CM nanoprobe. The merged images in Fig. 3d show that the Ag₂S@CM nanoprobe were targeted to the tumor site. Under the guidance of NIR II imaging, the electrical stimulation needles were inserted into the tumor.

Then the stimulation needles were connected to the fabric DC-TENG (as shown in Fig. 3e and Movie S2, Supporting Infor-

mation), and a 9 μ A pulsed current was applied to the tumor (Fig. 3f). The output of the fabric DC-TENG remains stable after 14 days treatment of tumor-bearing mice, which proves the outstanding durability of the device. (Fig. S8, Supporting Information). To optimize the distance between the two stimulation needles, the electric field around the stimulation needles was simulated by COMSOL software to evaluate the ablation area [11,50,53]. As shown in Fig. 3g, spherical tumor tissue with a diameter of 6 mm was constructed for the simulation. The simulation results show that the ablation area expanded significantly with the increase of the distance between the two needles. However, an excessively large spacing will result in a reduction in the effective ablation area. Therefore, the distance between the two stimulation needles was set to 3 mm to achieve the optimal triboelectric immunotherapy effect.

Immunological effects of electrical stimulation-induced dendritic cells recruitment

As an antigen-presenting cells (APCs), dendritic cells play an important role in the uptake and presentation of tumor antigens [51,54]. Considering the release of DAMPs driven by ICD of cells, numerous dendritic cells will be recruited to aggregate at tumor sites, take up tumor-associated antigens and migrate to TDLNs [54,55]. Afterwards, dendritic cells present antigens to T cells by expressing major histocompatibility complex II (MHC-II), initiating T cell-mediated adaptive immunity (Fig. 4a) [6,46]. Therefore, we investigated whether the electrical pulses generated by fabric DC-TENG can effectively achieve the recruitment and maturation of dendritic cells *in vivo*. Importantly, vascular damage to tissues by electrical stimulation was also explored. H&E staining images of tumor areas (48 h after stimulation) show that tumor cells of electrical stimulation-ablated tumor regions exhibited pyknosis and nuclear rupture (Fig. 4b), which are irreversible condensation of chromatin in nuclei undergoing apoptosis. Notably, the blood vessels in both control and power groups maintained intact structures, proving that electrical pulses of fabric DC-TENG did not damage the blood vessels. These properties allow dendritic cells to follow blood flow to the tumor site after electrical stimulation, significantly increasing the infiltration of dendritic cells in the tumor (Fig. 4d). Especially, infiltrating dendritic cells can migrate into TDLNs after ingesting relevant antigens [47]. Immunofluorescence staining of TDLNs sections was used to characterize the status of dendritic cells that migrated into TDLNs (Fig. S3, Supporting Information). Quantitative results indicate that the content of co-stimulatory molecules CD80/CD86 and antigen-presenting molecule MHC-II expressed by mature dendritic cells in TDLNs treated with electrical stimulation increased significantly, which could promote T cell activation (Fig. 4c). Furthermore, Flow cytometry (FCM) was also used to assess the electrical stimulation-induced immunological effects on promoting dendritic cells maturation and antigen presentation (Fig. 4e) [46,48]. The results further demonstrate that prolonged electrical stimulation triggers higher levels of dendritic cells maturation, resulting in a significant increase (39.0%) in the expression of CD80/CD86 in TDLNs.

Then, the adaptive immunity mediated by electrical stimulation-activated cytotoxic T cells was further validated. Notably, during the immune process in which mature den-

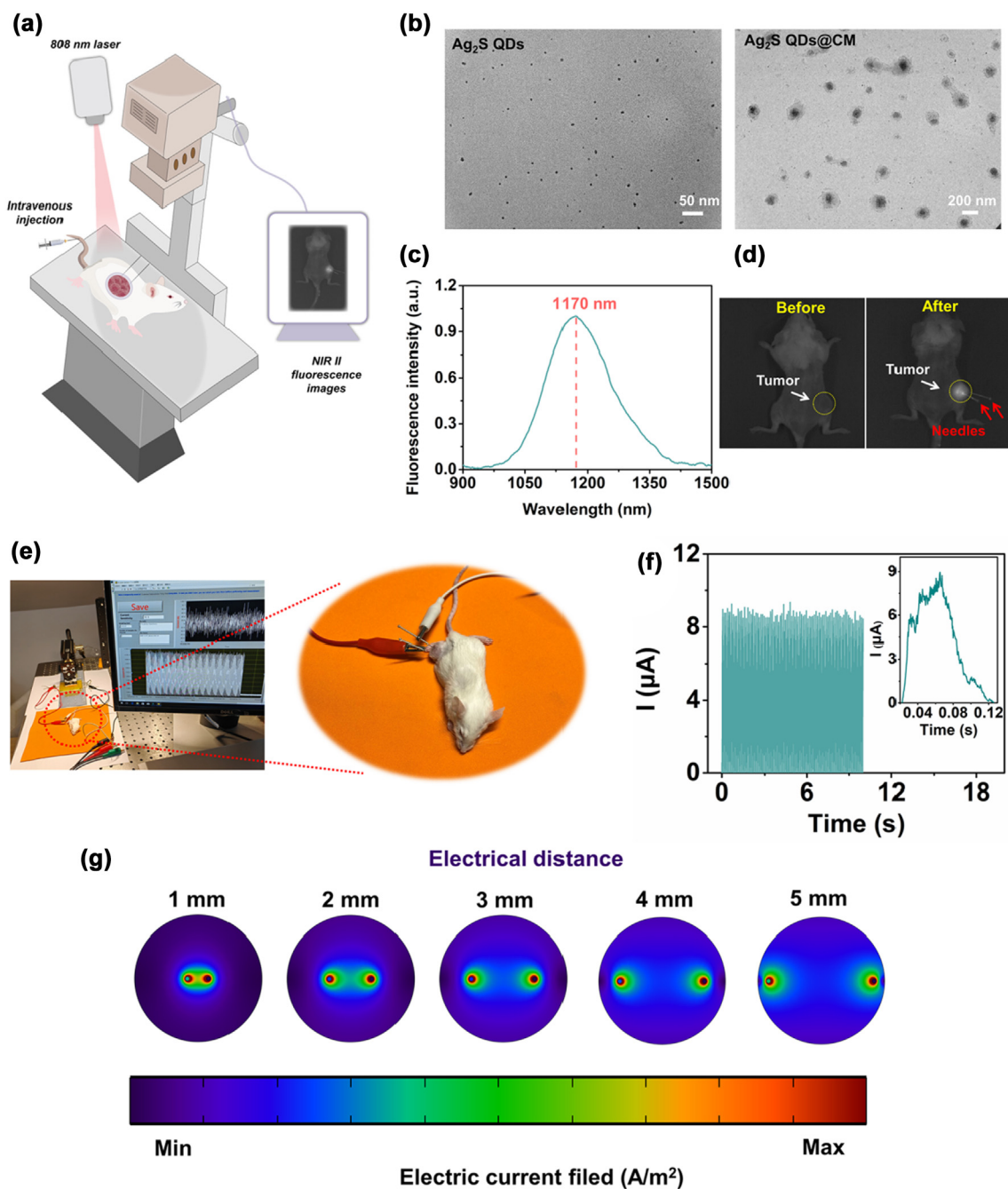


FIGURE 3

Imaging-guided triboelectric immunotherapy in solid tumor therapy. (a) Schematic diagram of electrical stimulation needle insertion under the guidance of NIR II fluorescence imaging. (b) TEM images of Ag₂S QDs and Ag₂S@CM nanoprob. (c) Normalized fluorescence emission spectrum of Ag₂S@CM nanoprob. (d) NIR II fluorescence images of 4T1 tumor-bearing mice before and after intravenous injection of Ag₂S@CM nanoprob (5 mg kg⁻¹) for 4 h. The yellow dotted line marks the tumor area, and the red arrow indicates the location of needle insertion. Light source: 808 nm, power density: 50 mW cm⁻². (e) The photograph of the experimental setup of the triboelectric immunotherapy system in tumor-bearing mice. (f) Currents flowing through tumors in tumor-bearing mice during electrical stimulation. Inset: a zoom image of single cycle current. (g) Electric current field images of tumor sites at different electrode implantation distances simulated by finite element method (FEM). Current intensity: 9 μA. Needle diameter: 0.1 mm.

drific cells present tumor-associated antigens and co-stimulatory molecules to T cells, T cells are activated to differentiate into highly cytotoxic CD4⁺ and CD8⁺ T cells, and infiltrate into tumor tissue along blood vessels (Fig. 5a) [51,54,56]. As shown in Fig. 5b, immunofluorescence staining of tumor tissues from 4T1 tumor-bearing mice (48 h after electrical stim-

ulation) demonstrates that fabric DC-TENG powered electrical stimulation resulted in massive recruitment of CD4⁺ and CD8⁺ T cells to tumor sites. At the same time, levels of granzyme B and perforin increased significantly at the tumor site (Fig. S9, Supporting Information), which are key cytokines that kill tumor cells. Additionally, a series of cytokines are released

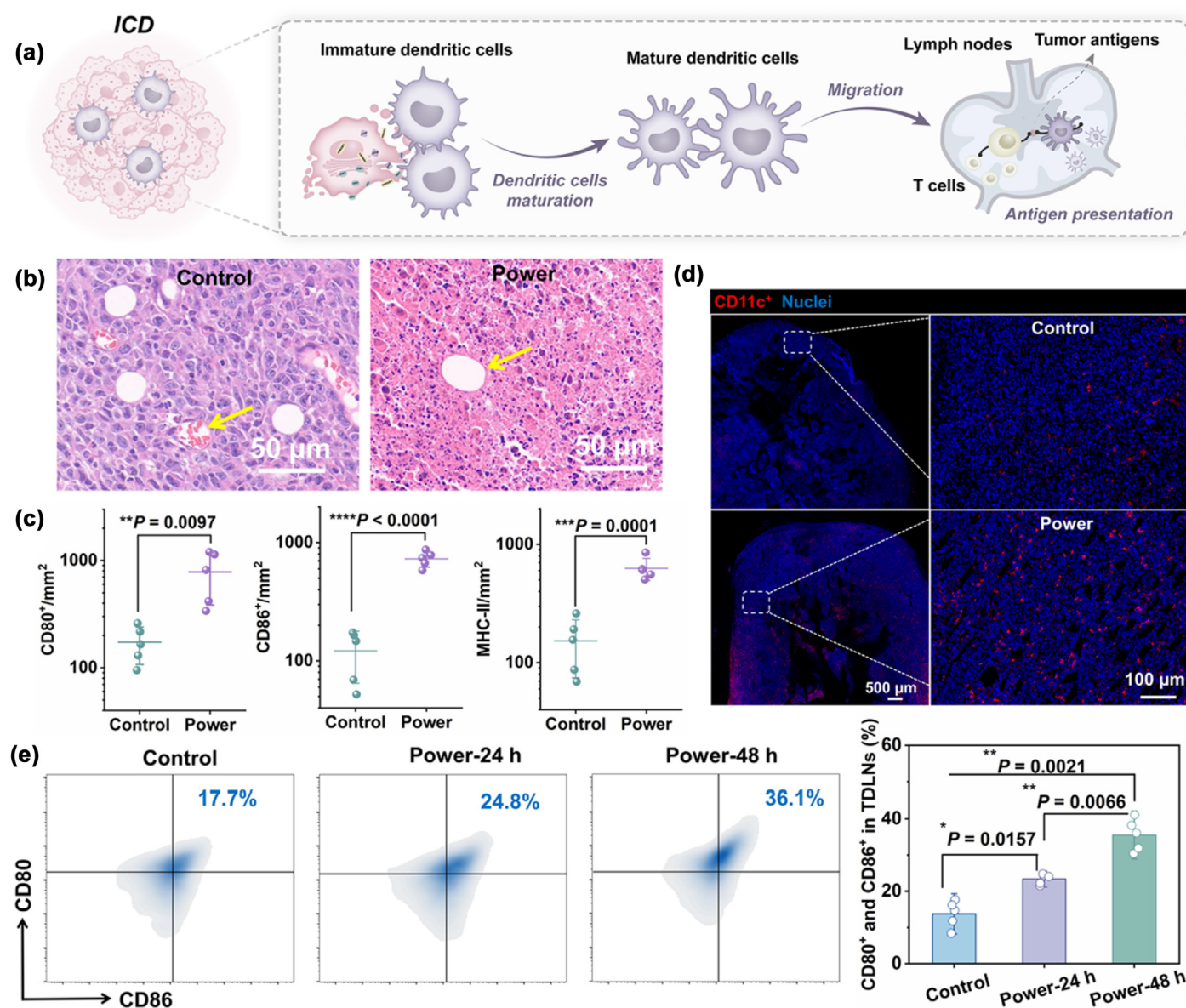


FIGURE 4

Fabric DC-TENG-driven electrical stimulation-promoted dendritic cells maturation and recruitment. (a) Schematic illustration of ICD-driven release of several DAMPs to facilitate antigen uptake and presentation by dendritic cells. (b) Representative H&E staining images of tumor areas in the control and power group. The yellow arrows mark the location of the venous vessels. (c) Corresponding quantitative histogram of immunofluorescence staining of CD80⁺/CD86⁺/MHC-II in representative TDLNs after 14 days of different treatment. Five fields of view in TDLNs are randomly captured. (d) Immunofluorescence staining of CD11c⁺ cells in tumor tissue of control group and power group. (e) Representative FCM analysis of CD80, CD86 in TDLNs and corresponding histograms of quantitative analysis. All data are presented as the mean values with error bars (standard deviations, \pm s.d.) from five biologically independent samples ($n = 5$). The statistical significance analysis was determined using Student's t-test (two-group analysis) or one-way analysis of variance (ANOVA) (multigroup analysis). n.s. not significant, $*p < 0.1$, $**p < 0.01$, $***p < 0.001$, $****p < 0.0001$.

and reach tumor tissue with blood circulation, among which tumor necrosis factor- α (TNF- α), interferon- γ (IFN- γ), and interleukin (IL)-2 and IL-12, are another important indicator of immune response [39,48,51]. The changes of cytokine content in tumor tissue at different times after electrical stimulation were measured by ELISA (Fig. 5c-f). The results show that the content of cytokines in tumor site decreased slightly within 2 h of ablation. The possible reason is that when electrical stimulation damages tumor cells, it may also damage immune cells, so the cytokine content decreases slightly in a short period of time. However, electrical stimulation damages cells with intact

cell membranes, and has little effect on some elastic tissues (eg, inner and outer elastic lamina, adventitia) [4,5]. Therefore, with the revascularization of blood vessels at a later stage, immune cells were recruited to the tumor site in large numbers, resulting in an enhanced immune response, which reached the highest level after 24 h (Fig. 5c-f). All these evidences suggest that electrical stimulation powered by fabric DC-TENG can significantly enhance the ICD of tumor cells, promote the recruitment of extensive dendritic cells and cytotoxic T cells (CD4⁺/CD8⁺) at tumor sites, and ultimately activate the adaptive immune system to fight tumors.

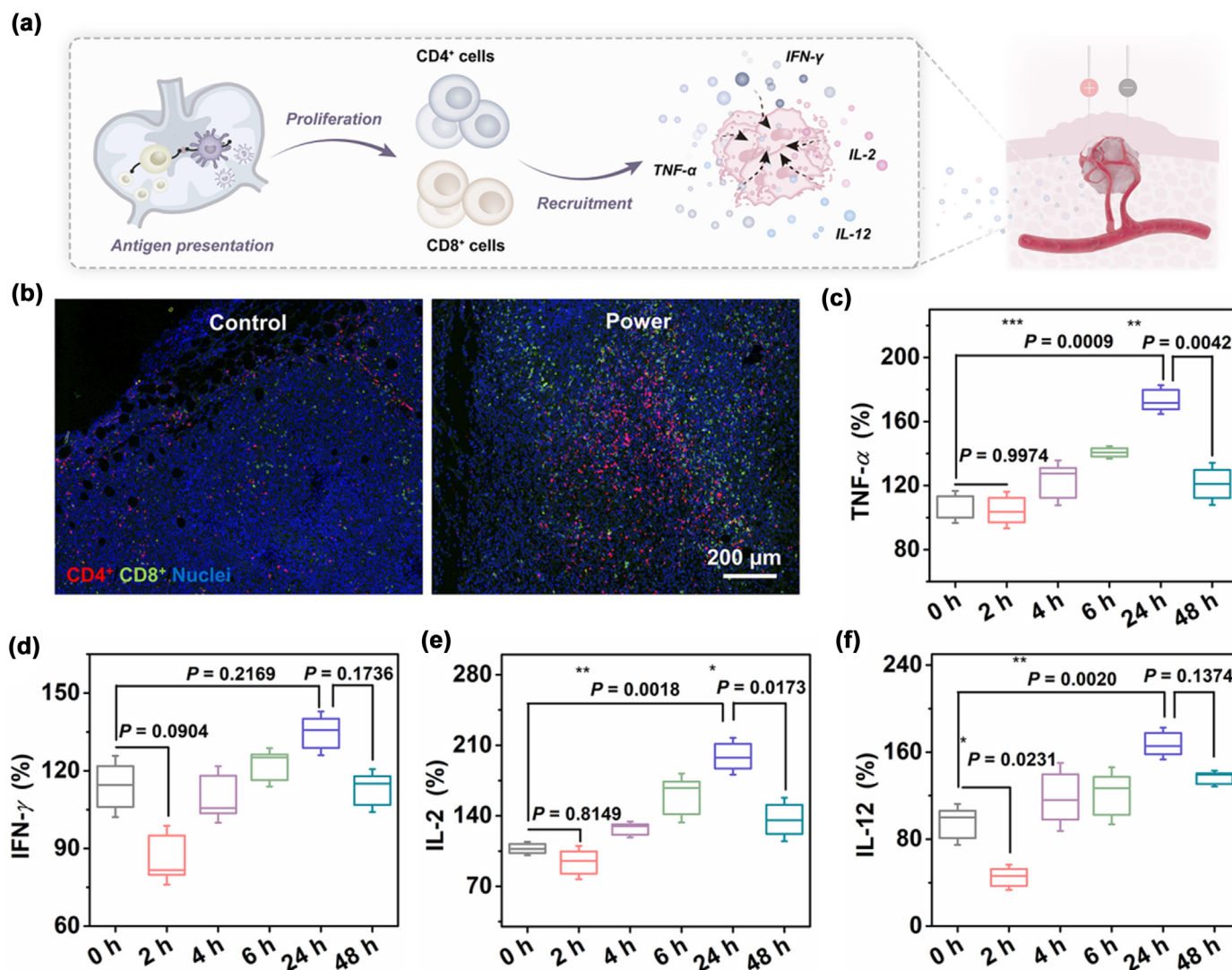


FIGURE 5

Electrical stimulation-induced T cell immune activation. (a) Schematic illustration of cytotoxic T cell differentiation and recruitment to tumor sites. (b) Representative immunofluorescence images of the distribution of CD4⁺/CD8⁺ T cells in the tumor tissues of the control group and therapy group after 14 days. (c-f) The percentages of cytokines (c) TNF- α , (d) IFN- γ , (e) IL-2, and (f) IL-12 in the tumors of mice at different times after electrical stimulation for 10 min. Tumors of mice were collected for ELISA analysis after 0 h, 2 h, 4 h, 6 h, 24 h, and 48 h. All data are presented as the mean values with error bars (standard deviations, \pm s.d.) from three biologically independent samples ($n = 3$). The statistical significance analysis was determined using Student's t-test (two-group analysis) or one-way analysis of variance (ANOVA) (multigroup analysis). n.s. not significant, * $p < 0.1$, ** $p < 0.01$, *** $p < 0.001$, **** $p < 0.0001$.

Antitumor therapeutic performance evaluation of triboelectric immunotherapy in vivo

The therapeutic performance of triboelectric immunotherapy was evaluated in tumor-bearing mice. As shown in Fig. 6a, electrical stimulation was performed for 10 min every two days, and the mice were sacrificed after 14 days of treatment. The results show that the body weight of the mice in each group did not change significantly during the treatment period (Fig. S10, Supporting Information). Interestingly, the growth of tumor, including volume and weight, were significantly inhibited in the power group relative to the control group (Fig. 6b-d). The mice survival curves within 58 days indicate that inhibition of tumor growth by electrical stimulation extended the lifespan of mice relative to the control group (Fig. 6e). For better understanding the therapeutic performance of pulsed direct-current from fabric DC-

TENG, the electrical stimulation treated tumor tissue is divided into ablation zone, transition zone and non-ablation zone (as shown in Fig. 6f). These zones can be observed correspondingly in the H&E staining images of tumor tissue. As shown in Fig. 6g, the ablation zone is clearly demarcated from the surrounding non-ablation zone. Distinct from the regular and dense cell morphology in the non-ablation zone, the tumor cells in the ablation zone are severely damaged, the nucleus disappeared, and the cells were fragmented [38,39,49]. Fabric DC-TENG-mediated tumor killing was then further characterized by other histological analyses (TUNEL staining and Ki67 immunohistochemical staining) (Fig. 6h) [39,57]. Similar to the results of H&E staining, TUNEL stained tumor sections after electrical stimulation show stronger green fluorescence, indicating that electrical stimulation can induce more significant apoptosis of tumor

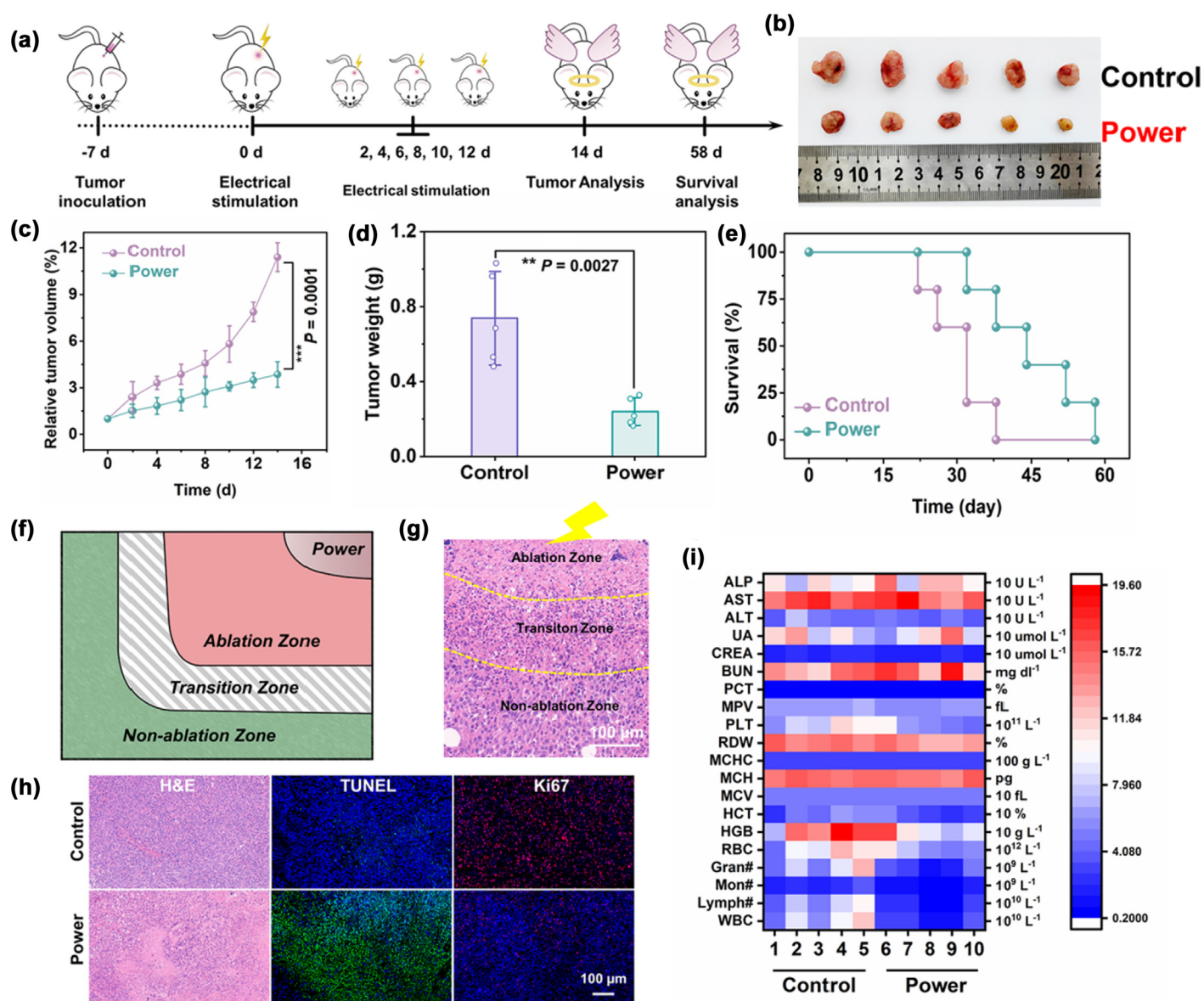


FIGURE 6

Triboelectric immunotherapy for 4T1 tumor-bearing mice. (a) Schematic illustration of the experimental protocol. (b) Photographs of tumors from individual mice, (c) relative tumor growth curves, (d) tumor weight histogram, and (e) mice survival curves (within 58 days) of control and power group. (f) Schematic illustration of ablation zone in tumor tissue. (g) Representative H&E staining image of tumor tissue 48 h after electrical stimulation. (h) Representative microscopic images of H&E, TUNEL, Ki67 staining of tumor ablation areas. (i) Heatmap of hematological analysis and serum biochemical analysis of individual mice after 14 days of treatment. All data are presented as the mean values with error bars (standard deviations, \pm s.d.) from five biologically independent samples ($n = 5$). The statistical significance analysis was determined using Student's t-test (two-group analysis) or one-way analysis of variance (ANOVA) (multigroup analysis). n.s. not significant, $*p < 0.1$, $**p < 0.01$, $***p < 0.001$, $****p < 0.0001$.

cells. The results of Ki67 staining further demonstrated that the tumor growth in the treated mice was effectively inhibited. These data confirm that the fabric DC-TENG driven triboelectric immunotherapy exhibits excellent tumor suppressive ability, which is a promising drug-free tumor ablation technique, especially for unresectable primary lesions.

Biosafety research of fabric DC-TENG-driven triboelectric immunotherapy

After 14 days of treatment, the liver and kidney function indexes of the mice were all within the normal range, which preliminar-

ily demonstrated the excellent biological safety of fabric DC-TENG-driven triboelectric immunotherapy. Notably, hematological analysis shows that the treated mice have lower white blood cell (WBC) values than the control group (Fig. 6i) [39,51,57]. Moreover, the results of organ coefficient represented that the spleen coefficient of mice after electrical stimulation is significantly lower than that of the control group (Fig. S11, Supporting Information), which denoted that triboelectric immunotherapy treatment can improve the obvious inflammatory symptoms of mice. The H&E staining images of the main organs of the mice in different treatment groups revealed that there was no obvious

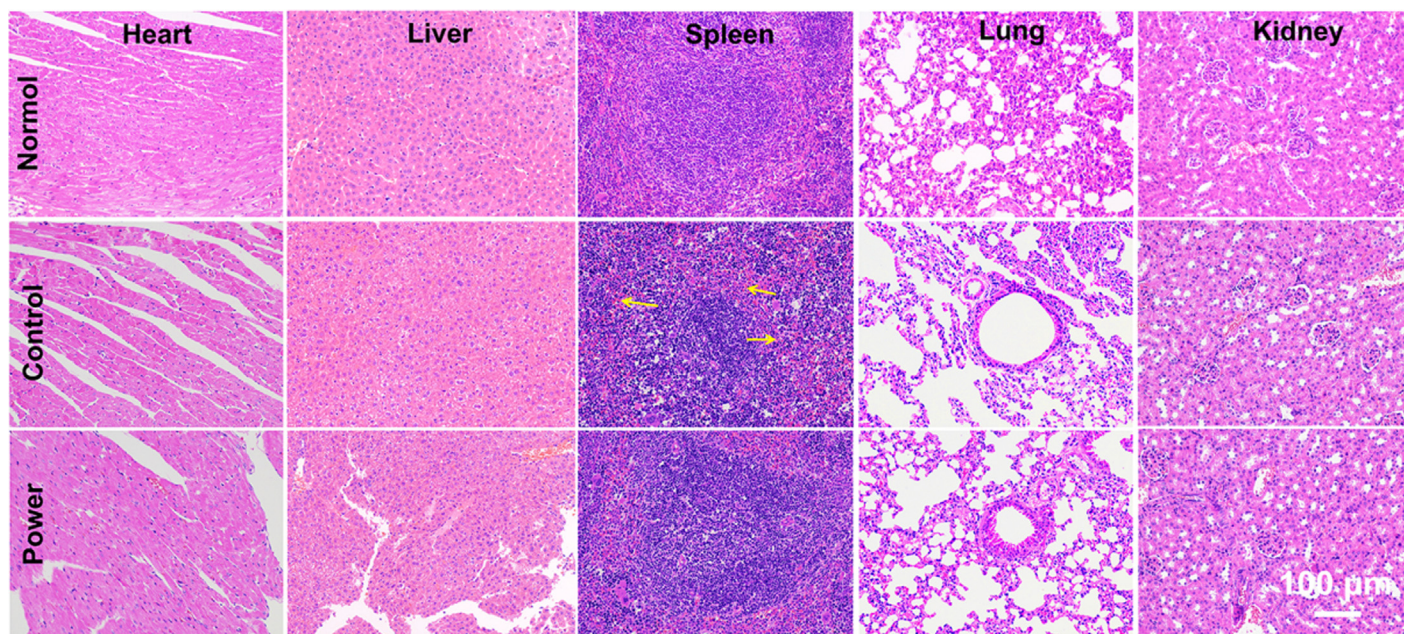


FIGURE 7

Representative H&E staining images of the heart, liver, spleen, lung and kidney of normal mice, tumor-bearing mice, and treated mice.

necrosis of the heart, liver, lungs and kidneys after treatment for 14 days. Importantly, the spleen of the mice in the control group was congested, while electrical stimulation treatment improved the organ lesions caused by cancer in the tumor-bearing mice (Fig. 7). These results demonstrate the excellent biosafety and therapeutic performance of fabric DC-TENG-driven triboelectric immunotherapy.

Conclusion

In summary, a promising drug-free triboelectric immunotherapy tumor ablation technique was developed by applying a pulsed direct-current generated from the coupled triboelectrification effect and electrostatic breakdown effect. Our results demonstrate that a small fabric DC-TENG (6.8 cm × 7 cm) can generate sufficiently high DC output to directly immunogenic cell death of 4T1 tumor cells. After electrical stimulation induced immunogenic cell death of tumor cells, massive tumor antigens and damage-associated molecular patterns are released, recruiting a large quantity of immune cells and APCs to aggregate at tumor site, inducing dendritic cells to mature and migrate to TDLNs to present tumor antigens to T cells. Subsequently, the activated T cells differentiate into cytotoxic CD4⁺ and CD8⁺ T cells, and secrete massive cytokines along with the blood and lymphatic vessels to infiltrate the tumor area, further inhibiting the tumor growth. The fabric DC-TENG driven triboelectric immunotherapy exhibits excellent tumor suppressive ability without the risks of drug toxicity, serious adverse reactions, strong drug dependence, and drug interaction of drug-related therapies, and significantly prolongs the survival period of the 4T1 tumor-bearing mice. Furthermore, the DC-TENG is composed of flexible textile, and can generate sufficiently strong currents in small dimensions without operation risks associated with high voltages in conventional power supplies, making triboelectric immunotherapy sys-

tem promising for next-generation miniaturized wearable tumor treatment devices.

Experimental section

Electric field simulation by finite element method

The electric field generated in the tumor when the TENG works was simulated according to the reported method. The preset tumor ablation area is a circular object with a diameter of 6 mm and a conductivity of 0.125 S/m. The simulated needle-like analog inserted into the electrode is 0.1 mm in diameter and has a metal conductivity of 4×10^6 . The electrode was inserted into the center of the tissue, the current value applied at both ends was 9 μ A, and the distance between the two electrodes was recorded as 1 mm, 2 mm, 3 mm, 4 mm, and 5 mm of ablation area.

Cell culture section

4T1 tumor cells (murine breast cancer cells) were a gift from Tongji Hospital of Huazhong University of Science and Technology. Cryopreserved cells were recovered with RPMI-1640 medium. Unless otherwise specified, 1 mL of medium contains 10 % fetal bovine serum and 1 % treptomycin/penicillin, and was kept at 37 °C in an incubator with continuous supply of 5 % CO₂. Incubate with fresh medium daily to ensure cells remain in optimal condition. Well-formed 4T1 cells were trypsinized and transferred to electroporation cups at a density of 1×10^6 cells/mL. The electroporation cups were connected to the two ends of the electrode, and the electrical stimulation of the cell was realized by the pulse current generated by the friction between the fabric DC-TENG and the PTFE plate.

Cell viability assay

Incubate the cells after electrical stimulation for 2 min, 5 min, 8 min, and 10 min in a 96-well plate at density of 4×10^3

cells/well for 24 h, then MTT reagent was added, and then measure the cell viability according to the method provided by the manufacturer.

The cell viability assay at different incubation times was similar to the above, except that the time of electrical stimulation was fixed for 10 min, and the cells were incubated in a 96-well plate for 2 h, 4 h, 6 h, 8 h, 24 h, and 48 h, and then MTT reagent was added to measure the cell viability. Friction distance: 50 mm, interval time: 0 s.

Cytoskeleton analysis of electrical stimulation effects

The cells after electrical stimulation for 10 min were placed in RPMI-1640 medium for 2 h to determine the recovery of reversibly electroporated cells. Cell slides were then prepared and the cytoskeleton was stained with the phalloidin according to the manufacturer's protocol. Stained pictures were recorded by SP8 Leica confocal laser scanning microscopy (Germany).

Electrical stimulation-mediated expression of DAMPs in cell

The electrically stimulated cells (Stimulation time: 10 min) were made into cell slides at a density of 1×10^6 cells/well. Cells were incubated overnight with CRT (Cat 12238, 1:200) and HMGB1 (Cat ab18256, 1:200) as primary antibodies according to the manufacturer's protocol. Then, cells were covered with corresponding secondary antibodies (1 h, 25 °C), and nuclei were stained with DAPI (G1012, Servicebio). Fluorescence microscopy (Nikon Eclipse C1, Japan) and imaging systems (Nikon DS-U3, Japan) are used for image of cells.

Electrically stimulated cells (Stimulation time: 10 min) were seeded in 6-well plates for 12 h. The cell culture medium after incubation for 24 h and 48 h was taken, and the extracellular HMGB1 was measured by HMGB1 ELISA kit (E-EL-MO676c) according to the method provided by the manufacturer. ATP secreted by cells was measured by ATP detection kit (S0027).

Construction of tumor-bearing mice model

The 5-week-old Balb/c mice were purchased from the Hubei Provincial Laboratory Animal Research Center. A tumor-bearing mouse model was established by subcutaneously inoculating 1×10^6 4T1 cells in the right leg of the mice. When the tumor volume developed to 100 mm³, the mice were randomly divided into the control group and the power group ($n = 5$). The mice in the power group were anesthetized with isoflurane gas before treatment. The electrodes were made of medical grade stainless steel needles, and electrical stimulation with a duration of 10 min was applied every two days. The treatment period was 14 days, and data such as body weight and tumor size of the mice were recorded during the treatment period.

Fluorescence imaging in vivo

The detailed synthetic scheme of Ag₂S@CM is shown in the [Supporting Information](#). The Ag₂S@CM nanoprobes were intravenously injected into tumor-bearing mice. After 4 h of circulation *in vivo*, the mice were anesthetized with isoflurane gas, and the imaging of the nanoprobes in the mice was recorded using a NIR-II Small Animal Imaging System (series II 900/1700, China).

Immunofluorescence staining analysis

The mice after 14 days of treatment were euthanized, and the tumors were taken for H&E, TUNEL, Ki67, CD11c⁺, CD4⁺, CD8⁺ immunohistochemistry and immunofluorescence staining. Tumor-draining lymph nodes removed from mice for CD80/CD86/MHC-II immunofluorescence staining. Anti-CD11c (1:300, GB11059), Anti-CD4 (1:200, ab183685), Anti-CD8 (1:200, GB13429), Anti-CD80 (1:200, bs-2211R), Anti-CD86 (1:100, GB13585), anti-MHC-II (1:200, bs-4107R). Fluorescence microscopy was used for imaging, and results were quantified by Image J software.

Flow analysis and ELISA analysis of cytokines

Tumors of mice in each experimental group were digested into cell suspension, and the content of cytokine (TNF- α , IFN- γ , IL-2, IL-12) in tumors was detected by ELISA detection kit according to the method provided by the manufacturer.

The TDLNs of the mice were removed and trypsinized for 1 h to prepare cell suspensions. Undigested cell pellets were filtered through a 40 μ m nylon mesh. Markers of dendritic cells maturation: CD86/FITC (1:200, rat, clone 3D5, bsm-30162A-FITC), CD80/PE (1:200, rat, clone 8H2, bsm-30264A-PE). Stained cells were recorded using a flow cytometer (FACS Calibur, BD), and flowjo software was used for statistical analysis of the data.

Data and materials availability

All data are available in the main text or the [supplementary materials](#).

CRediT authorship contribution statement

Haimei Li: Methodology, Visualization, Data curation, Investigation, Writing – original draft, Writing – review & editing. **Chaoyu Chen:** Methodology, Visualization, Data curation, Investigation, Writing – original draft, Writing – review & editing. **Zichen Wang:** Formal analysis, Methodology, Data curation. **Yiman Huang:** Data curation, Investigation. **Guangqin He:** Methodology, Data curation, Investigation. **Yi Liu:** Funding acquisition, Supervision, Conceptualization, Validation, Writing – original draft, Writing – review & editing. **Peng Jiang:** Funding acquisition, Supervision, Conceptualization, Project administration, Software, Writing – original draft, Writing – review & editing. **Zhong Lin Wang:** Funding acquisition, Supervision, Conceptualization, Resources, Writing – original draft, Writing – review & editing.

Data availability

Data will be made available on request.

Declaration of Competing Interest

The authors declare that they have no known competing financial interests or personal relationships that could have appeared to influence the work reported in this paper.

Acknowledgements

This research was supported by the National Natural Science Foundation of China (22074113, 22073070), Science and Technology Plans of Tianjin (22ZYJDS00070), the Young Top-

notch Talent Cultivation Program of Hubei Province, and the Large-scale Instrument and Equipment Sharing Foundation of Wuhan University (LF20221381). All animal experiments were approved by the Institutional Animal Care and Use Committee (IACUC) of the Animal Experiment Center of Wuhan University (Wuhan, China). All animal experiments involved strictly abide by the Regulations for the Administration of Affairs Concerning Experimental Animals formulated by the State Council of the People's Republic of China.

Appendix A. Supplementary material

Supplementary data to this article can be found online or from the author. Supplementary data to this article can be found online at <https://doi.org/10.1016/j.mattod.2023.02.026>.

References

- [1] N.N. Zhang et al., *Front. Immunol.* 12 (2022), <https://doi.org/10.3389/fimmu.2021.811726> 811726.
- [2] B. Geboers et al., *Radiology* 295 (2020) 254–272, <https://doi.org/10.1148/radiol.2020192190>.
- [3] S.W. Zhao, A.S. Mehta, M. Zhao, *Cell. Mol. Life Sci.* 77 (2020) 2681–2699, <https://doi.org/10.1007/s00018-019-03446-1>.
- [4] Y. Kong et al., *Adv. Sci.* 8 (2021) 2100962, <https://doi.org/10.1002/advs.202100962>.
- [5] Z.G. Liu et al., *World J. Gastroenterol.* 26 (2020) 3421–3431, <https://doi.org/10.3748/wjg.v26.i24.3421>.
- [6] B.J. Wang et al., *Small* 18 (2022) 2201056, <https://doi.org/10.1002/smll.202201056>.
- [7] F. Babikr et al., *Cell. Mol. Immunol.* 18 (2021) 2632–2647, <https://doi.org/10.1038/s41423-021-00796-4>.
- [8] W.F. Zhang et al., *Adv. Funct. Mater.* 435 (2022) 2203029, <https://doi.org/10.1002/adfm.202203029>.
- [9] G.C. Li et al., *Adv. Sci.* 8 (2021) 2100964, <https://doi.org/10.1002/advs.202100964>.
- [10] J.H. Han et al., *Small* 18 (2022) 2200316, <https://doi.org/10.1002/smll.202200316>.
- [11] E.J. Go et al., *Cancers* 12 (2020) 3123, <https://doi.org/10.3390/cancers12113123>.
- [12] B.J. Burbach et al., *Nat. Commun.* 12 (2021) 3862, <https://doi.org/10.1038/s41467-021-24132-6>.
- [13] V. Novickij et al., *Cancers* 11 (2019) 1763, <https://doi.org/10.3390/cancers11111763>.
- [14] H.M. Peng et al., *Adv. Sci.* 9 (2022) 2105240, <https://doi.org/10.1002/advs.202105240>.
- [15] J.H. Han et al., *Biomaterials* 289 (2022), <https://doi.org/10.1016/j.biomaterials.2022.121762> 121762.
- [16] R.E. Neal et al., *J. Clin. Oncol.* 31 (2013) e422–e426, <https://doi.org/10.1200/JCO.2012.44.9736>.
- [17] C.Y. Calvet, L.M. Mir, *Cancer Metast. Rev.* 35 (2016) 165–177, <https://doi.org/10.1007/s10555-016-9615-3>.
- [18] S.K. Frandsen, M. Vissing, J. Gehl, *Cancers* 12 (2020) 290, <https://doi.org/10.3390/cancers12020290>.
- [19] F. Collettini et al., *Radiology* 292 (2019) 250–257, <https://doi.org/10.1148/radiol.2019181987>.
- [20] S.X. Sun et al., *Cancer Lett.* 502 (2021) 9–24, <https://doi.org/10.1016/j.canlet.2020.12.018>.
- [21] P.J. Hosein et al., *J. Clin. Oncol.* 30 (2012) 291, https://doi.org/10.1200/jco.2012.30.4_suppl.291.
- [22] J.S. Guo et al., *Bioelectrochemistry* 123 (2018) 26–33, <https://doi.org/10.1016/j.bioelechem.2018.04.010>.
- [23] J. Rogers, Z.N. Bao, T.W. Lee, *Acc. Chem. Res.* 52 (2019) 521–522, <https://doi.org/10.1021/acs.accounts.9b00048>.
- [24] X.D. Chen et al., *Chem. Soc. Rev.* 48 (2019) 1431–1433, <https://doi.org/10.1039/c9cs90019e>.
- [25] F.R. Fan, Z.Q. Tian, Z.L. Wang, *Nano Energy* 1 (2012) 328–334, <https://doi.org/10.1016/j.nanoen.2012.01.004>.
- [26] C.S. Wu et al., *Adv. Energy Mater.* 9 (2019) 1802906, <https://doi.org/10.1002/aenm.201802906>.
- [27] Q. Zheng et al., *Sci. Adv.* 2 (2016) e1501478, <https://doi.org/10.1126/sciadv.1501478>.
- [28] X. Guo et al., *Nano Energy* 92 (2022), <https://doi.org/10.1016/j.nanoen.2021.106762> 106762.
- [29] R. Hinchet et al., *Science* 365 (2019) 491–494, <https://doi.org/10.1126/science.aan3997>.
- [30] C.S. Wu et al., *Adv. Funct. Mater.* 30 (2020) 1907378, <https://doi.org/10.1002/adfm.201907378>.
- [31] Y. Long et al., *ACS Nano* 12 (2018) 12533–12540, <https://doi.org/10.1021/acsnano.8b07038>.
- [32] Z.R. Liu et al., *Adv. Mater.* 31 (2019) 1807795, <https://doi.org/10.1002/adma.201807795>.
- [33] D. Liu et al., *Sci. Adv.* 5 (2019) eaav6437, <https://doi.org/10.1126/sciadv.aav6437>.
- [34] S.Y. Chen et al., *Adv. Mater. Techno.* 6 (2021) 2100195, <https://doi.org/10.1002/admt.202100195>.
- [35] C.Y. Chen et al., *ACS Nano* 14 (2020) 4585–4594, <https://doi.org/10.1021/acsnano.0c00138>.
- [36] Z.H. Zhao et al., *Nano Energy* 102 (2022), <https://doi.org/10.1016/j.nanoen.2022.107745> 107745.
- [37] W.S. Boyle, P. Kisliuk, *Phys. Rev.* 97 (1955) 255, <https://doi.org/10.1103/physrev.97.255>.
- [38] J.T. Xu et al., *Adv. Funct. Mater.* 28 (2018) 1803804, <https://doi.org/10.1002/adfm.201803804>.
- [39] H.M. Li et al., *Anal. Chem.* 94 (2022) 10470–10478, <https://doi.org/10.1021/acs.analchem.2c01738>.
- [40] D. Hendriks et al., *Nat. Protoc.* 16 (2021) 182–217, <https://doi.org/10.1038/s41596-020-00411-2>.
- [41] B.B. Chu et al., *Nano Energy* 100 (2022), <https://doi.org/10.1016/j.nanoen.2022.107471> 107471.
- [42] C.S. Szot et al., *Biomaterials* 32 (2011) 7905–7912, <https://doi.org/10.1016/j.biomaterials.2011.07.001>.
- [43] T. Polajzer, T. Jarm, D. Miklavcic, *Radiol Oncol.* 54 (2020) 317–328, <https://doi.org/10.2478/raon-2020-0047>.
- [44] C.B. He et al., *Clin. Transl. Med.* 10 (2020) e39, <https://doi.org/10.1002/ctm2.39>.
- [45] M.J. Zhang et al., *Adv. Mater.* 34 (2022) 2205701, <https://doi.org/10.1002/adma.202205701>.
- [46] W.C. Wu et al., *Nano Today* 42 (2022), <https://doi.org/10.1016/j.nantod.2022.101377> 101377.
- [47] Y.F. Yin et al., *Nano Today* 36 (2021), <https://doi.org/10.1016/j.nantod.2020.101009> 101009.
- [48] H.N. Zhao et al., *ACS Nano* 15 (2021) 13188–13199, <https://doi.org/10.1021/acsnano.1c02765>.
- [49] H.N. Zhao et al., *Chem. Eng. J.* 394 (2020), <https://doi.org/10.1016/j.cej.2020.124314> 124314.
- [50] Y. Zhang et al., *Radiology* 256 (2010) 424, <https://doi.org/10.1148/radiol.10091955>.
- [51] H. Li et al., *Nat. Commun.* 12 (2021) 7149, <https://doi.org/10.1038/s41467-021-27485-0>.
- [52] P. Jiang et al., *Biomaterials* 33 (2012) 5130–5135, <https://doi.org/10.1016/j.biomaterials.2012.03.059>.
- [53] C.K. Sung et al., *Technol. Cancer Res. Treat.* 16 (2017) 488–496, <https://doi.org/10.1177/1533034616640642>.
- [54] W. Xie et al., *ACS Nano* 16 (2022) 10742–10753, <https://doi.org/10.1021/acsnano.2c02605>.
- [55] H.Q. Chen et al., *Biomaterials* 269 (2021), <https://doi.org/10.1016/j.biomaterials.2020.120639> 120639.
- [56] B.C. Wei et al., *Nano Lett.* 21 (2021) 4231–4240, <https://doi.org/10.1021/acs.nanolett.1c00209>.
- [57] Y.F. Liu et al., *ACS Appl. Mater. Interfaces* 13 (2021) 60933–60944, <https://doi.org/10.1021/acsmi.1c20486>.